Thermal conductivity of interfacial layers in nanofluids

Zhi Liang and Hai-Lung Tsai[*]

[1]*Department of Mechanical and Aerospace Engineering, Missouri University of Science and Technology, Rolla, Missouri 65409, USA*

Thermal conductivity of interfacial layers is an essential parameter for determining how the ordered liquid layering around the particle-liquid interface contributes to the unusual high thermal conductivity of nanofluids. However, so far there is no experimental data regarding this parameter. Using nonequilibrium molecular dynamics simulations of an inhomogeneous Au-Ar system in which the solid-liquid interactions are assumed to be much stronger than the liquid-liquid interactions, we show explicitly that the thermal conductivity of a 1-nm-thick interfacial layer is $1.6 \sim 2.5$ times higher than that of the base fluid. The simulation results are incorporated into a three-level clustering model to calculate the effective thermal conductivity of nanofluids. The results show that the contribution of the interfacial layer to thermal conductivity enhancements should be considered if there are particle clusters in nanofluids.

PACS number(s): 68.08.De, 66.25.+g, 82.70.Dd

I. INTRODUCTION

As a new class of heat-transfer fluid, nanofluids (nanoscale colloidal suspensions) have attracted increasing attention, primarily due to their greatly enhanced thermal conductivities as compared to those of their base fluids. Although the thermal conductivity enhancement (TCE) of most nanofluids can be successfully predicted by the classical Maxwell's theory for well-dispersed spherical nanoparticles [1], some experimental observations show enhanced thermal conductivity beyond the prediction of Maxwell's theory [2–6]. Recent reviews [4,7,8] concerning the thermal conductivity of nanofluids have extensively discussed the possible mechanisms leading to this "unusual" TCE. This subject has been hotly debated over the past decade, and various models in favor of or against different mechanisms have been proposed. Similar to other proposed mechanisms, such as ballistic phonon transport in nanoparticles and the Brownian motion of nanoparticles, enhancement due to the larger thermal conductivity of the ordered interfacial liquid layer around solid surfaces is also a controversial issue, mainly for two reasons: (1) Despite that there are various theoretical models [9–12] that take into account the influence of interfacial layers on the effective thermal conductivity of nanofluids, there is no experimental data regarding an essential parameter for these theoretical models, which is the thermal conductivity of the interfacial layer k_{il} [8]. Researchers have to make assumptions for the thermal conductivity as well as the thickness h of the interfacial layer in order to verify the proposed theoretical models and the interfacial layer TCE mechanism. Although some of the experimental data can be fitted with these models, the assumptions of k_{il} and h in many cases are questionable. (2) Using molecular dynamics (MD) simulations, Xue *et al.* showed that the interfacial layer has no effect on thermal transport [13], while Eapen *et al.* showed that a strong solid-liquid interaction can induce a percolating network of thermal conduction paths mediated by the interfacial fluid atoms [14,15]. Although the TCE beyond the Maxwell limit shown in the results of Eapen *et al.* were obtained for a

nanofluid consisting of exceedingly small colloidal particles (a few tens of atoms), their results do imply that the thermal conductivity of the interfacial layer is higher than that of the base fluid.

Recently, a nuclear magnetic resonance (NMR) experiment was performed to study layering of water molecules on the surface of alumina nanoparticles [16]. It was estimated from the NMR experiment that the thickness of the ordered layer is around 1.4 nm. Since the mean separation between the nanoparticles in a common nanofluid is much larger than the estimated thickness of the ordered layer, a percolating network of interfacial layer cannot be formed for well-dispersed particles. According to the renovated Maxwell model developed by Yu and Choi [9], such a thin interfacial layer has a very small impact on nanofluid thermal conductivity if the particle size is a few tens of nanometers. However, several recent theoretical and experimental studies strongly suggested that nanoparticle clustering plays a significant role in the thermal transport in nanofluids [6,17–21]. According to these studies, local high particle concentrations due to the clustering of nanoparticles may exist, which strongly increases the probability of inducing a percolating network of interfacial layers. When applying the effective medium theory (EMT) model to the calculation of the effective thermal conductivity of nanofluids, however, these studies did not consider the contribution from the interfacial layer. If the percolating network of interfacial layers is induced by particle clustering, the interfacial layer may have non-negligible enhancement effects on the effective thermal conductivity of the cluster, which consequently enhances the effective thermal conductivity of the whole nanofluid. Therefore the effect of the interfacial layer needs to be included in a clustering model to determine if it is appropriate to ignore the contribution from the interfacial layer.

To consider the effect of the interfacial layer, the main challenge is to find the thermal conductivity k_{il} and thickness h of the interfacial layer [8]. These two parameters, especially k_{il}, are difficult to obtain from experiments and have not been explicitly determined from MD simulations so far. In this paper, we first develop a nonequilibrium MD model to evaluate the thermal conductivity and thickness of the interfacial liquid layer. Specifically, the layering of liquid Ar on the Au surface is studied. The calculated k_{il} and h are the essential parameters

———————
[*]Corresponding author: tsai@mst.edu
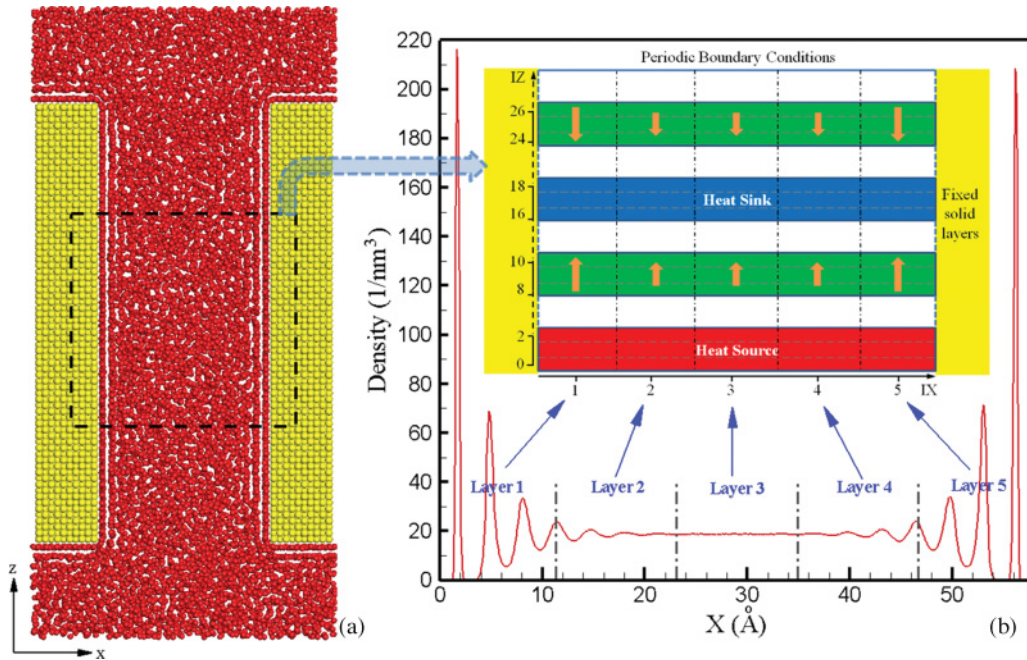
FIG. 1. (Color online) (a) Structure of a typical Au-Ar system in the MD simulation. (b) Density distribution of liquid Ar between Au walls in the x direction for base liquid at 150 K and 18.61/nm^3. The inset is a schematic diagram of an Au-Ar system for nonequilibrium MD simulation. Liquid Ar is divided evenly into five layers.

for the subsequent EMT model, which incorporates the effect of the interfacial layer in a three-level effective medium clustering model developed by Prasher *et al.* [17]. We find that the contribution from the interfacial layer to the enhancement of effective thermal conductivity should not be neglected when it is combined with the particle clustering effects.

II. MOLECULAR DYNAMICS MODEL

To calculate the thermal properties of the interfacial liquid layer, we first study the structure and density variation of the fluid close to a solid-liquid interface by conducting an equilibrium MD simulation of two parallel planar Au walls immersed in a liquid Ar reservoir at a temperature of 150 K and an atomic number density of 18.61/nm^3 ($\sim$31 mol/L). As shown in Fig. 1, both the Au walls consist of [1 0 0]-oriented perfect face-centered cubic (fcc) crystal of lengths $5a_0$ in the x direction, $8a_0$ in the y direction, and $36a_0$ in the z direction, where $a_0 = 4.079$ Å is the lattice constant of Au [22]. The width of the fluid between two parallel walls is 5.79 nm. Periodic boundary conditions (PBCs) are applied in three directions. The Ar-Ar interaction is modeled by Lennard-Jones (LJ) 12-6 potential with the parameters $\sigma = 3.41$ Å and $\varepsilon = 119.8$ K [23]. The Ar-Au interaction is also modeled by LJ potential. To obtain interaction parameters, $\sigma_S = 2.569$ Å and $\epsilon_S = 5313$ K are used for Au [24]. The Lorentz-Berthelot mixing rule is employed to calculate the LJ parameters for Ar-Au interactions. The cutoff radius for all interactions is 2.5σ. We integrate the equations of motion using a velocity Verlet scheme with a 2-fs time step size. The Berendsen *et al.* algorithm [25] with a 0.6-ps time constant is used to equilibrate the system to 150 K. To be consistent with the subsequent nonequilibrium MD simulation for the thermal conductivity

of the interfacial layer, Au atoms are fixed at perfect crystal positions during the simulation. The density of liquid Ar in the reservoir is maintained at 18.61/nm^3 during the equilibration. After a 500-ps initialization period, the density distribution of liquid Ar becomes steady. Figure 1 shows the variation of Ar density in the x direction within a dashed region of $16a_0$ length in the z direction. It is found that the density profile oscillates over 2 nm from the solid-liquid interface due to the liquid layering and then becomes a constant which is equal to the density of the base fluid. However, it does not necessarily mean that the thickness of the interfacial liquid layer is about 2 nm. Figures 2(a)–2(d) show the in-plane radial distribution functions (RDFs) within a 1.7-Å-thick plane centered at various x locations corresponding to the first four density peak locations shown in Fig. 1. It is evident that the in-plane structure changes from crystalline structure to liquid-like structure within 1 nm. After this distance, the RDFs are indistinguishable from the in-plane RDF of the base fluid, which is shown in Fig. 2(e). Therefore it is more reasonable to take the thickness of the interfacial fluid layer as about 1 nm, which mainly includes the first three density peaks as shown in Fig. 1. Accordingly, we divide the liquid Ar between the two solid surfaces evenly into five layers (1.158 nm each layer). The two layers most adjacent to the solid surfaces are considered as interfacial layers. Nonequilibrium MD simulation is applied to determine the thermal conductivity of each fluid layer.

In the nonequilibrium MD simulation, we focus on heat flow in the z direction, which is parallel to the solid surface. The solid and liquid structures in the primary simulation cell are reproduced from the equilibrium structures of liquid and solid in the dashed region shown in Fig. 1. To evaluate possible finite size effects in the MD simulation of thermal conductivity [26], the system size in the z direction is varied
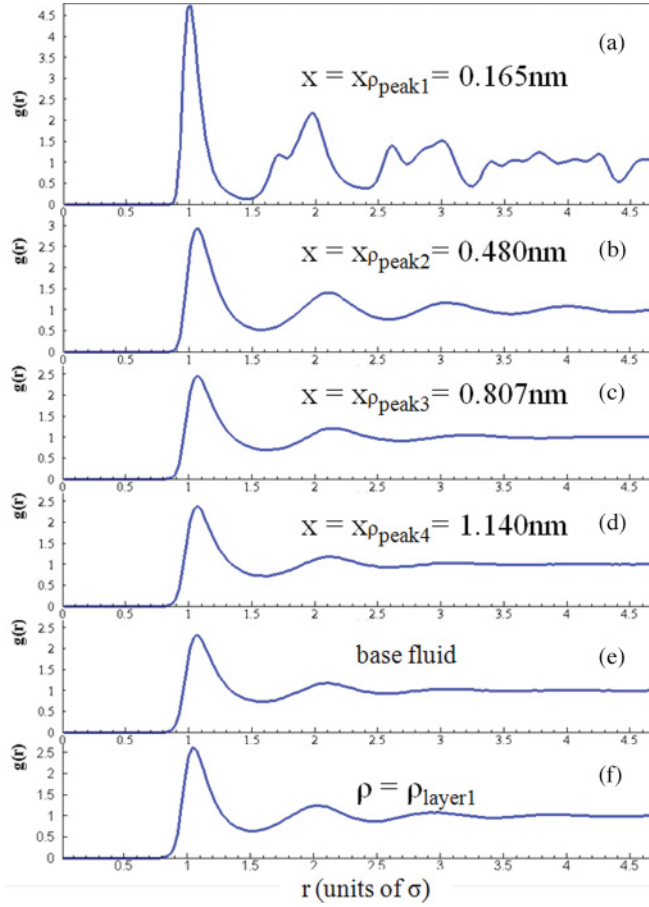
FIG. 2. (Color online) (a)–(d) In-plane RDFs [$g(r)$] centered at different x locations in liquid Ar between Au walls. (e) In-plane RDF of the homogeneous base fluid. (f) In-plane RDF of a homogeneous bulk fluid with density equal to the average density of the interfacial layer. In $g(r)$, the distance from a given atom at (x_0, y_0, z_0) is calculated as $r = \sqrt{(y - y_0)^2 + (z - z_0)^2}$.

from $64a_0$ (26.1 nm) to $96a_0$ (39.2 nm) by reproducing the primary simulation cell ($16a_0$ long in the z direction) four to six times and connecting these reproduced cells one after another in the z direction. As illustrated in the inset of Fig. 1, PBCs are applied in both the y and z directions. Au atoms are fixed during the simulation since we study only the heat flow in liquid layers. Liquid Ar is divided evenly into 32 bins in the z direction. Bins 0–2 belong to the heat source region. Bins 16–18 belong to the heat sink region. Bins 8–10 and 24–26 belong to the heat flux measurement region. A constant energy ΔE is added to the energy of atoms in the heat source region and subtracted from the energy of atoms in the heat sink region at each time step so that the total energy of the system is conserved during the simulation. Note that the liquid Ar in the simulation cell is an inhomogeneous fluid system. If the conventional velocity scaling method which scales the velocities of all atoms in the heat source or heat sink region with the same factor is employed, it is possible to produce nonzero temperature gradients in the x direction in addition to that in the z direction, which makes the calculation of thermal conductivity complicated. In this work, therefore, the heat source and heat sink regions are both evenly divided

into five subregions, as shown in Fig. 1. At each time step, we first calculate a nominal temperature of the whole heat source or heat sink region by $T = (E_K \pm \Delta E)/\frac{3}{2}Nk_B$, where E_K and N are, respectively, the total kinetic energy and total number of atoms in the heat source or heat sink region, and k_B is the Boltzmann constant. Then the velocities of the atoms in each subregion are scaled with a factor to make the temperature of each subregion reach the nominal temperature T. Since the instantaneous total kinetic energy of the atoms in each subregion differs from one another, the scaling factors for different subregions are different. Using this approach, the possible temperature difference between the neighboring subregions is eliminated and the total energy of the simulation system is still conserved during the simulation. Additionally, the conservation of total momentum of the system is ensured during the velocity scaling process by using the Jude and Jullien's method [27]. As shown in the inset of Fig. 1, the heat flux measurement region is also divided into five subregions which correspond to five liquid layers. To evaluate the average heat flux $\bar{q}$ in each subregion, the following equation is used for the calculation [28]:

$$\bar{q} = \frac{1}{V}\left[\sum_i E_i \, \vec{v}_i + \frac{1}{2}\sum_i\sum_j \vec{r}^*_{ij}(\vec{v}_i \cdot \vec{F}_{ij})\right] \qquad (1)$$

In Eq. (1), V is the volume of a heat flux measurement subregion, E_i is the sum of the kinetic energy and potential energy of atom i, $\vec{v}_i$ is the velocity of atom i, and $\vec{F}_{ij}$ denotes the interatomic force. The first term on the right side of Eq. (1) is a summation over all atoms in the subregion. The double summation in the second term is over all pairs of atoms, with the condition that the line connecting the two atoms is contained or partially contained in the subregion. Accordingly, $\vec{r}^*_{ij}$ in Eq. (1) is the whole connecting vector or the portion of the connecting vector contained in the subregion. The heat fluxes in the x, y, and z directions are all calculated during the simulation.

Each nonequilibrium MD simulation starts with a 6-ns initial period to let the systems reach a steady state. Subsequently, a 150-ns period is used for data collection and averaging. At every time step, the temperatures in the 32 bins of each fluid layer and heat flux in each heat flux measurement subregion are calculated. Due to the long simulation length, the statistical uncertainties of temperature and heat flux are about $\pm 0.1\%$ and $\pm 1.5\%$, respectively. Figure 3 shows the calculated temperature profiles in the z direction of the five liquid Ar layers for a $96a_0$-long simulation system. We can see from Fig. 3 that the temperature profiles in the five liquid layers are all identical, which indicates that there exist only nonzero temperature gradients in the z direction. In the heat source and sink region, a parabolic shape of temperature profile is observed, which is consistent with the PBCs. Between these two regions, the temperature profile is almost linear. With the identical temperature gradient ($dT/dz \approx 1.71\,\text{K/nm}$), the liquid layer with higher thermal conductivity should show larger heat flux. As shown in Fig. 4, q_z in the two interfacial layers (layer 1 and layer 5) is higher than that in the middle layers, while q_x and q_y in all liquid layers are almost zero, as expected. Based on the simulation results shown in Figs. 3 and 4, the
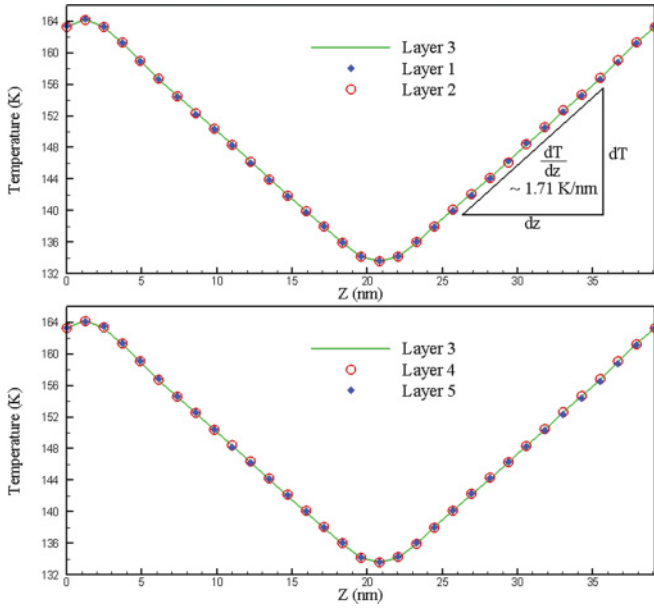
FIG. 3. (Color online) The temperature profiles in different liquid layers in the z direction.

thermal conductivity of different liquid layers k_{layer} can be readily calculated by Fourier's law. As shown in Fig. 5, k_{layer} of the middle three layers is about 0.10 W/m K, while the k_{layer} of the interfacial layers, i.e., k_{il}, is about 0.16 W/m K. In Fig. 4 we also show the average density of each liquid layer. The density of the middle liquid layers is found to be almost the same as the density of the base liquid, while the density of the interfacial layers is about 17% higher than that of the base liquid.

To investigate whether the higher thermal conductivity of the interfacial layers is caused simply by the higher density, a similar nonequilibrium MD simulation is carried out to calculate the thermal conductivity of a homogeneous bulk Ar liquid at a density equal to that of the different liquid layers and at a temperature of 150 K. The calculation results are shown
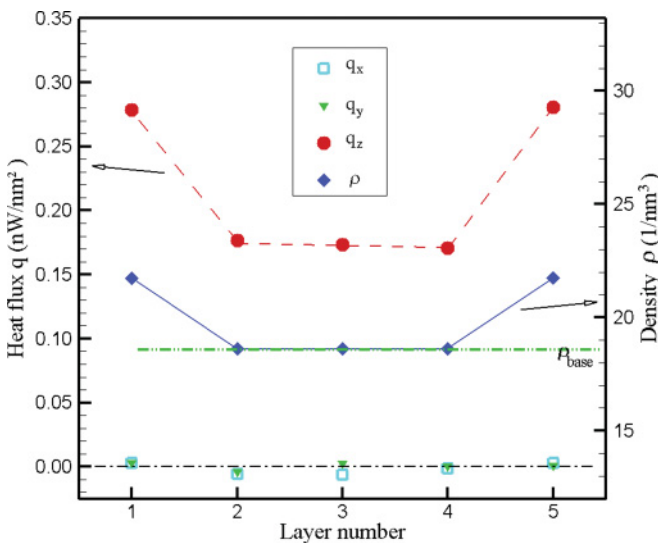
FIG. 4. (Color online) The heat flux and average density in different liquid layers.
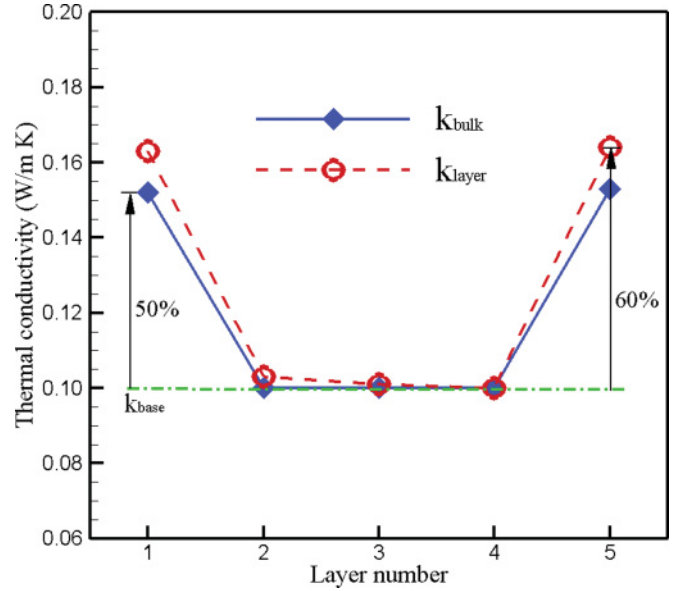
FIG. 5. (Color online) The thermal conductivity of different liquid layers k_{layer} and the thermal conductivity of homogeneous bulk fluids k_{bulk} with the density and temperature of the same values as those in the corresponding liquid layers.

in Fig. 5. The difference between the thermal conductivity of the middle liquid layers and the thermal conductivity of bulk liquid at the same density and temperature is found generally within statistical uncertainties. Hence neither the density nor the thermal conductivity of the middle liquid layers is affected by the solid walls, which further confirmed that the thickness of the interfacial liquid layer is limited to about 1 nm. On the other hand, the thermal conductivity of a bulk liquid having the same density as the interfacial layer is found to be lower than that of the interfacial layer. As depicted in Fig. 5, $(k_{il} - k_{\text{base}})/k_{\text{base}} \times 100\% \approx 60\%$, while at the same temperature and density, $(k_{\text{bulk}} - k_{\text{base}})/k_{\text{base}} \times 100\% \approx 50\%$. As suggested by Evans *et al.* [29], a fluid with a more ordered structure may have a higher thermal conductivity even when the same fluid density is maintained. We calculate the in-plane RDF of the bulk liquid and show the result in Fig. 2(f). Compared to the RDFs of the interfacial layer [mainly Figs. 2(a)–2(c)], the structure of the bulk liquid is slightly more ordered than the structure shown in Fig. 2(c), but evidently less ordered than the structures shown in Fig. 2(a), which has the feature of the crystalline structure, and shown in Fig. 2(b), which has the feature of the solid-liquid coexistence structure. Hence the overall fluid structure in the interfacial layer is more ordered than that of a bulk liquid at the same density and temperature. The extra 10% enhancement of thermal conductivity should come from more ordered structure in the interfacial layer. We further investigate whether the TCE in the interfacial layer is affected by the system size in the z direction. No discernible effect is observed for a system size from 26.1 to 39.2 nm, which implies that the mean free path of phonons in the interfacial layer is much less than the system size, and size effect is not significant in this simulation. From the simulation of an Au-Ar system, therefore, we know $k_{il} \approx 1.6\,k_{\text{base}}$ and that the enhancement is mainly due to the enhanced density of
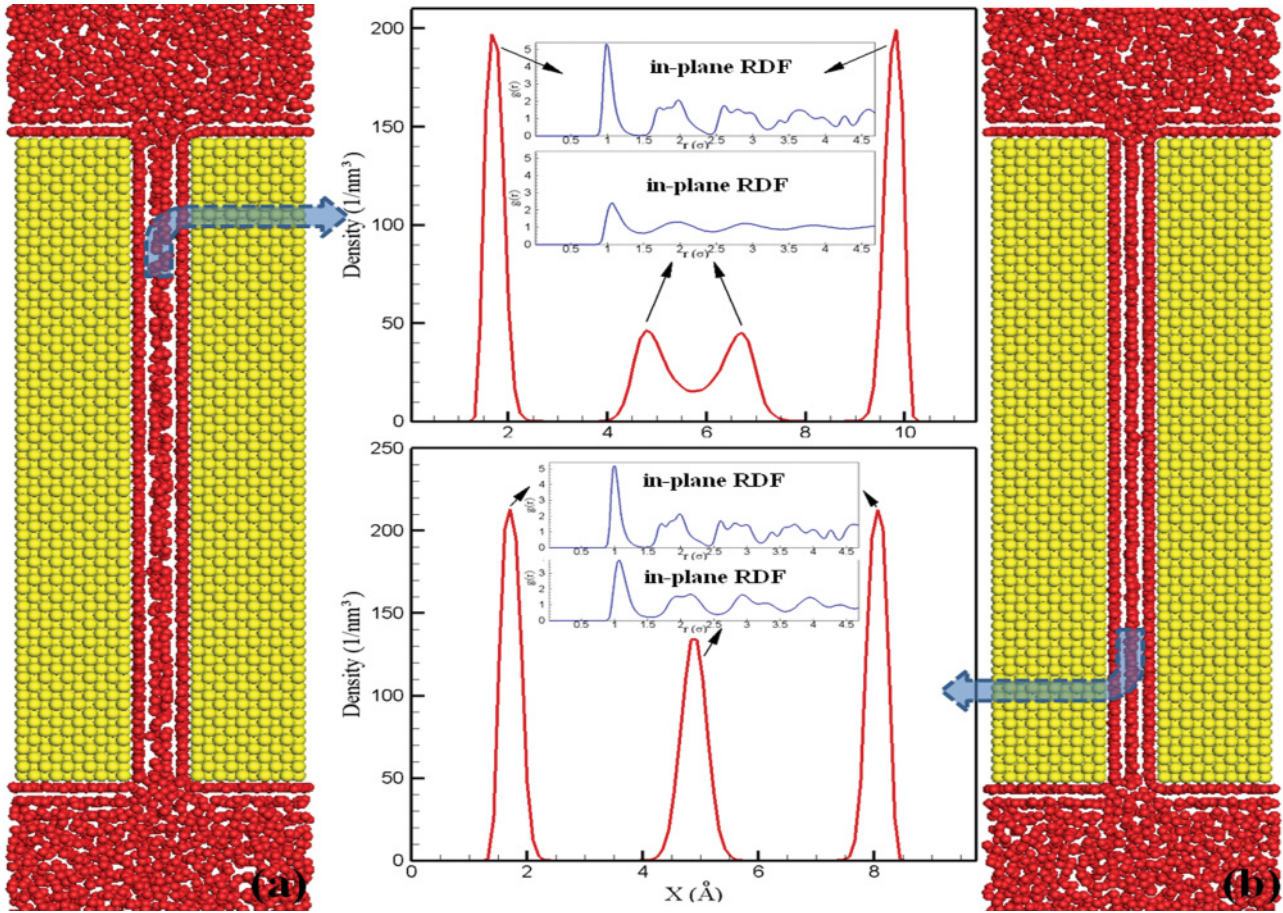
FIG. 6. (Color online) Snapshot of Au-Ar system, density distribution of Ar between Au walls in the x direction, and in-plane RDFs centered at locations corresponding to different density peaks for base liquid at 150 K and 18.61/nm³. (a) Separation of Au walls equals 1.158 nm. (b) Separation of Au walls equals 0.978 nm.

the interfacial layer and partially due to the more ordered fluid structure.

For a well-dispersed nanofluid of low particle volume fraction, the separation between two particles is normally much larger than the thickness of the interfacial layer. Due to Brownian motion and clustering effects, however, particles might be locally very close to each other, likely on the order of the thickness of the interfacial layer [30]. We now investigate how the small interparticle separation affects the thermal conductivity of the interfacial layer. First we reduce the separation between two solid walls to 1.158 nm, which is the same as the thickness of the interfacial liquid layer in the previous simulation. The base fluid is still maintained at 150 K and 18.61/nm³. A similar MD simulation as mentioned above is performed to calculate the equilibrium density and structure of the fluid between solid walls. Figure 6(a) shows a snapshot of this Au-Ar system in equilibrium. Four density peaks are observed within the thin Ar layer. The average density of the thin Ar layer is 23.54/nm³, which is about 26.5% higher than the density of the base fluid. In the calculation of thermal conductivity, the thin Ar layer was not divided into more sublayers and the length of the simulation cell was 26.1 nm. Using nonequilibrium MD simulation, we find the thermal conductivity of this 1.158-nm thin Ar layer is $k_{layer} = 0.218$ W/m K, which is 118% higher than $k_{base} =$

0.10 W/m K, while the thermal conductivity of a bulk Ar fluid at the same density and temperature is $k_{bulk} = 0.193$ W/m K, which is 93% higher than k_{base}. The extra 25% enhancement comes from the more ordered structure in the thin Ar layer. Compared to the property of the interfacial liquid layer in the large interparticle separation case, the small separation between particles induces an even higher average fluid density and more ordered fluid structure, which results in a further enhancement of thermal conductivity.

When the separation between two solid walls is further reduced to 0.978 nm, the middle two density peaks merge into one sharp density peak, as shown in Fig. 6(b). From the in-plane RDFs shown in the bottom-middle of Fig. 6, the Ar molecules between walls now form a molecular solid. At thermal equilibrium, the average density of this molecular solid is 26.61/nm³, which is 43.0% higher than the density of the base fluid. The thermal conductivity of the thin molecular solid is $k_{layer} = 0.248$ W/m K, which is 148% higher than k_{base}, while the thermal conductivity of a bulk Ar at the same density and temperature is $k_{bulk} = 0.246$ W/m K. At such a high density, a bulk Ar at 150 K also becomes a solid whose structure is almost as ordered as that of the thin molecular solid. Hence it is reasonable to find $k_{layer} \approx k_{bulk}$ in this case. We vary the length of the simulation cell from 26.1 to 52.2 nm to investigate the size effect of k_{layer}. No discernible variation

of k_{layer} is observed, which implies a rather imperfect crystal structure of the thin molecular solid and that the mean free path of phonons in the thin molecular solid is much smaller than the system size. The high enhancement of thermal conductivity in this case is almost all caused by the extremely high density.

According to the above MD simulation, therefore, we obtain the thickness of the interfacial layer, which is about 1 nm, and depending on the separation between the two solid surfaces, the thermal conductivity of interfacial liquid layer is $1.6 \sim 2.5$ times higher than that of the base fluid. In such a range of thermal conductivity and thickness, it has been proved that the enhancement of effective thermal conductivity of nanofluids due to the interfacial layer effect is small (only about 1% enhancement compared to the prediction of Maxwell's model for a 4% volume fraction of particles with radius of 16.5 nm) [12] for well-dispersed nanoparticles. In the following EMT model, we focus on a nanofluid containing nanoparticle clusters and study the influence of the interfacial layer on its effective thermal conductivity.

The thermal conductivity calculated in our MD model is the one parallel to the solid surface. The following EMT model, however, needs the thermal conductivity in both perpendicular and parallel directions. Since the interfacial layer includes only about three liquid layers, it is difficult to accurately evaluate the thermal conductivity of such a thin layer in the perpendicular direction from the MD model. In the following calculation we assume the thermal conductivity of the interfacial layer is the same in both directions.

III. EFFECTIVE MEDIUM THEORY MODEL

The EMT model used in this work is modified from a three-level clustering model developed by Prasher *et al.* that does not consider the interfacial layer effect [17]. Briefly, the model of Prasher *et al.* assumes a particle cluster is embedded within a sphere of radius R_g and the cluster spheres are uniformly distributed in the liquid. Each cluster is composed of a few approximately linear chains spanning the whole cluster, which is called the backbone of the cluster, and side chains which are called dead ends. The volume fractions of the nanoparticles, the backbone particles, and the dead-end particles in the cluster sphere are, respectively, $\phi_{\text{int}} = (R_g/a)^{d_f-3}$, $\phi_c = (R_g/a)^{d_l-3}$ and $\phi_{nc} = \phi_{\text{int}} - \phi_c$, where d_f and d_l are, respectively, the fractal dimension and chemical dimension. In this calculation, we assume $R_g = 5a$ and set $d_f = 1.8$ and $d_l = 1.4$, according to Prasher *et al.* [17]. Due to number conservation of the particles, $\phi_p = \phi_{\text{int}}\phi_a$, where ϕ_p and ϕ_a are the volume fraction of nanoparticles and cluster spheres in the liquid, respectively. After all these definitions, Prasher *et al.*'s model starts with the first level of homogenization, which is performed with only the particles belonging to the dead ends. The effective thermal conductivity of the cluster sphere in the presence of the dead-end particles only, k_{nc}, is determined by solving Eq. (2), which is based on the Bruggeman model [31]. The model is particularly suitable for composites with high-concentration additives and is given by

$$\phi_{nc}\left(\frac{k_p - k_{nc}}{k_p + 2k_{nc}}\right) + (1 - \phi_{nc})\left(\frac{k_{\text{base}} - k_{nc}}{k_{\text{base}} + 2k_{nc}}\right) = 0 \quad (2)$$

where k_p is the thermal conductivity of the nanoparticle. Equation (2) does not consider the interfacial layer effects. To take into account the influence of the interfacial layer, we consider each nanoparticle with radius of a to be covered with an interfacial layer of thickness h. The volume fraction of a nanoparticle in this structure, therefore, is $\phi_e = a^3/(a + h)^3$. The effective thermal conductivity of the particle-interfacial layer structure for dead-end particles, k_{ed}, can be obtained by solving Eq. (3) [11].

$$\frac{k_{ed}}{k_{il}} = \frac{k_p + 2k_{il} + 2\phi_e(k_p - k_{il})}{k_p + 2k_{il} - \phi_e(k_p - k_{il})} \quad (3)$$

Based on the MD simulation result, $k_{il} = 2k_{\text{base}}$ and $h = 1$ nm are used in the calculation; $k_p = 200k_{\text{base}}$ is assumed. To incorporate the effect of interfacial layer at this level, we modify Eq. (2) by replacing k_p and ϕ_{nc} in Eq. (2) by k_{ed} and ϕ_{nc}/ϕ_e, respectively.

In the second level of homogenization in Prasher's model, k_a, the effective thermal conductivity of the cluster sphere, including the particles belonging to the backbone, is calculated by assuming that the backbone is embedded in a medium with an effective thermal conductivity of k_{nc} obtained from Eq. (2). The model of Nan *et al.* [32] is used to calculate k_a by solving Eq. (4),

$$\frac{k_a}{k_{nc}} = \frac{3 + \phi_c[2\beta_{11}(1 - L_{11}) + \beta_{33}(1 - L_{33})]}{3 - \phi_c(2\beta_{11}L_{11} + \beta_{33}L_{33})} \quad (4)$$

where $L_{11} = 0.5p^2/(p^2 - 1) - 0.5p/(p^2 - 1)^{1.5} \cdot \cosh^{-1}p$, $p = R_g/a, L_{33} = 1 - 2L_{11}, \beta_{11} = (k_p - k_{nc})/[k_{nc} + L_{11}(k_p - k_{nc})]$, and $\beta_{33} = (k_p - k_{nc})/[k_{nc} + L_{33}(k_p - k_{nc})]$. Again, the interfacial layer is not taken into account at this level in Prasher's model. When the backbone is formed, the nanoparticles belonging to the backbone are so close to each other that the interfacial layers are connected to one another and form a percolating network. Thus by assuming the nanoparticles in the backbone are embedded in the interfacial layer medium, we can calculate the effective thermal conductivity of the backbone-interfacial layer structure k_e using the Bruggeman model.

$$\phi_e\left(\frac{k_p - k_e}{k_p + 2k_e}\right) + (1 - \phi_e)\left(\frac{k_{il} - k_e}{k_{il} + 2k_e}\right) = 0 \quad (5)$$

To incorporate the effect of the interfacial layer in Prasher's model at this level, k_e calculated from Eq. (5) and ϕ_c/ϕ_e should substitute k_p (in the expressions for β_{11} and β_{33}) and ϕ_c in Eq. (4), respectively.

Finally, k_{eff}, the effective thermal conductivity of the whole nanofluid, is calculated by the Maxwell-Garnet (MG) model [18].

$$\frac{k_{\text{eff}}}{k_{\text{base}}} = \frac{k_a + 2k_{\text{base}} + 2\phi_a(k_a - k_{\text{base}})}{k_a + 2k_{\text{base}} - \phi_a(k_a - k_{\text{base}})} \quad (6)$$

No modification is needed at this level to include the effect of the interfacial layer. Since k_a in Eq. (6) is obtained by solving Eq. (4), the change of k_a due to incorporating the effect of the interfacial layer in the previous two levels will result in a change of k_{eff} in Eq. (6). We vary the volume fraction of nanoparticles ϕ_p in the whole nanofluid from 0 to 0.05 and calculate the effective thermal conductivity of the whole
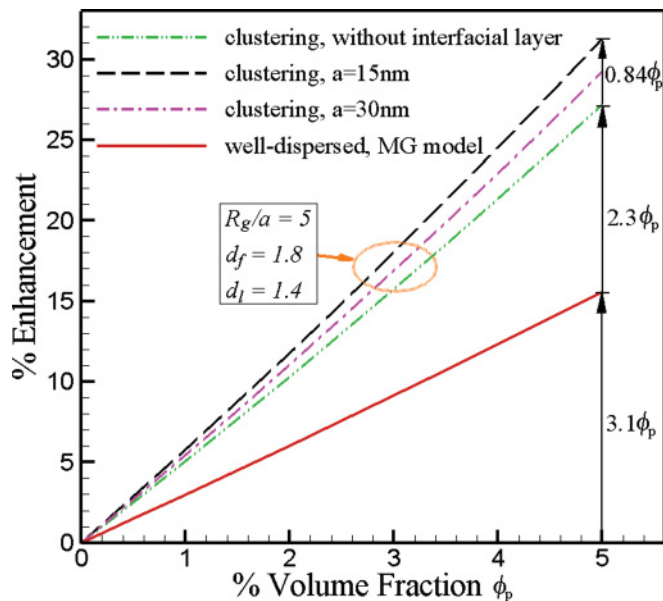
FIG. 7. (Color online) TCE in nanofluids as a function of particle volume fraction. The solid line is calculated using the MG model for a nanofluid with well-dispersed nanoparticles. The influence of the interfacial layer is not considered. The remaining lines are calculated using the clustering model. The influence of the interfacial layer is considered in the calculation of the dashed line results for particles with radius of 15 nm and dash-dot line results for particles with radius of 30 nm.

nanofluid k_{eff} using Prasher *et al.*'s model and our modified model to investigate the influence of the interfacial layer on k_{eff}. Thermal boundary resistance is neglected in the calculation. As shown in Fig. 7, the TCEs of a nanofluid with well-dispersed nanoparticles and a nanofluid containing particle clusters are 15.5% and 27.1%, respectively, for a 5% particle volume fraction. Both results neglect the influence of the interfacial layer. The enhancement is consistent with Prasher's results, which show that thermal conductivity can be significantly enhanced as a result of nanoparticle clustering. When the influence of the interfacial layer is incorporated, the thermal conductivity of a nanofluid with clusters is further enhanced to 29.2% and 31.3% for particles with radius of 30 and 15 nm, respectively.

The enhancement increases with deceasing particle size, as expected. As depicted in Fig. 7, the TCE predicted by the MG model is about $3.1\phi_p$. When the clustering effect is considered, a further enhancement of $2.3\phi_p$ is predicted by Prasher's model. If the interfacial layer effect is incorporated, an extra $0.84\phi_p$ TCE is observed for particles with radius of 15 nm. Therefore the influence of the interfacial layer should not be neglected in the clustering model, indicating that the clustering of particles gives a major contribution to the TCE in nanofluids.

IV. SUMMARY

In summary, we calculate the thickness and thermal conductivity of the interfacial liquid layer by MD simulations. Our results indicate that the enhancement of thermal conductivity of the interfacial layer is mainly caused by the increased density and partially caused by the more ordered structure. Although the interfacial layers with thickness of 1 nm and thermal conductivity of $1.6 \sim 2.5k_{\mathrm{base}}$ has only a small impact on the thermal conductivity of a nanofluid with well-dispersed nanoparticles, their contribution to TCE in a nanofluid containing particle clusters should not be neglected.

The simulation results shown in this paper correspond to a nanofluid with strong solid-liquid interactions. The thickness and thermal conductivity of interfacial liquid layers and their contribution to TCE are closely related to the strength of solid-liquid interactions. For many realistic systems which contain wetting interfaces, the solid-liquid interaction is about the same strength as liquid-liquid interactions. In these cases, the contribution to the TCE from an interfacial liquid layer may be smaller or disappear. Stronger solid-liquid interactions are therefore desirable in the manufacturing process of nanofluids in order to achieve higher effective thermal conductivity.

[1] P. Keblinski, J. A. Eastman, and D. G. Cahill, Mater. Today **8**, 36 (2005).

[2] J. A. Eastman, S. U. S. Choi, S. Li, W. Yu, and L. J. Thompson, Appl. Phys. Lett. **78**, 718 (2001).

[3] S. U. S. Choi, Z. G. Zhang, W. Yu, F. E. Lockwood, and E. A. Grulke, Appl. Phys. Lett. **79**, 2252 (2001).

[4] J. Eapen, R. Rusconi, R. Piazza, and S. Yip, J. Heat Transfer **132**, 102402 (2010).

[5] H. Zhu, C. Zhang, Y. Tang, and J. Wang, J. Phys. Chem. C **111**, 1646 (2007).

[6] J. W. Gao, R. T. Zheng, H. Ohtani, D. S. Zhu, and G. Chen, Nano Lett. **9**, 4128 (2009).

[7] P. Keblinski, R. Prasher, and J. Eapen, J. Nanopart. Res. **10**, 1089 (2008).

[8] S. Ozerinc, S. Karac, and A. Y. Guvenc, Microfluid. Nanofluid. **8**, 145 (2010).

[9] W. Yu and S. U. S. Choi, J. Nanopart. Res. **5**, 167 (2003).

[10] B. Wang, L. Zhou, and X. Peng, Int. J. Heat Mass Transfer **46**, 2665 (2003).

[11] Q. Xue and W. Xu, Mater. Chem. Phys. **90**, 298 (2005).

[12] E. Doroodchi, T. M. Evans, and B. Moghtaderi, J. Nanopart. Res. **11**, 1501 (2009).

[13] L. Xue, P. Keblinski, S. R. Phillpot, S. U. S. Choi, and J. A. Eastman, Int. J. Heat Mass Transfer **47**, 4277 (2004).

[14] J. Eapen, J. Li, and S. Yip, Phys. Rev. E **76**, 062501 (2007).

[15] J. Eapen, J. Li, and S. Yip, Phys. Rev. Lett. **98**, 028302 (2007).

[16] C. Gerardi, D. Cory, J. Buongiorno, L. Hu, and T. Mckrell, Appl. Phys. Lett. **95**, 253104 (2009).

[17] R. Prasher, W. Evans, P. Meakin, J. Fish, P. Phelan, and P. Keblinski, Appl. Phys. Lett. **89**, 143119 (2006).

[18] R. Prasher, P. E. Phelan, and P. Bhattacharya, Nano Lett. **6**, 1529 (2006).

[19] D. Lee, J. W. Kim, and B. G. Kim, J. Phys. Chem. B **110**, 4323 (2006).

[20] K. S. Hong, T. K. Hong, and H. S. Yang, Appl. Phys. Lett. **88**, 031901 (2006).

[21] Y. Xuan and W. Hu, AIChE J. **49**, 1038 (2003).

[22] F. Cleri and V. Rosato, Phys. Rev. B **48**, 22 (1993).

[23] G. C. Maitland, M. Rigby, E. B. Smith, and W. A. Wakeham, *Intermolecular Forces: Their Origin and Determination* (Clarendon Press, Oxford, 1981).

[24] P. M. Agrawal, B. M. Rice, and D. L. Thompson, Surf. Sci. **515**, 21 (2002).

[25] H. J. C. Berendsen, J. P. M. Postma, W. F. Van Gunsteren, A. Di Nola, and J. R. Haak, J. Chem. Phys. **81**, 3684 (1984).

[26] D. P. Sellan, E. S. Landry, J. E. Turney, A. J. H. McGaughey, and C. H. Amon, Phys. Rev. B **81**, 214305 (2010).

[27] P. Jund and R. Jullien, Phys. Rev. B **59**, 13707 (1999).

[28] T. Ohara, J. Chem. Phys. **111**, 9667 (1999).

[29] W. Evans, J. Fish, and P. Keblinski, J. Chem. Phys. **126**, 154504 (2007).

[30] J. A. Eastman, S. R. Phillpot, S. U. S. Choi, and P. Keblinski, Annu. Rev. Mater. Res. **34**, 219 (2004).

[31] D. A. G. Bruggeman, Ann. Phys. (Leipzig) **24**, 636 (1935).

[32] C.-W. Nan, R. Birringer, D. R. Clarke, and H. Gleiter, J. Appl. Phys. **81**, 6692 (1997).